Structural design, qualification and post-flight assessment of Crew Module Fairing

Nishant Singh, R. K. Sajeev, P. Ayyappadas, A. P. Beena* and C. K. Krishnadasan

Structural Engineering Entity, Vikram Sarabhai Space Centre, Thiruvananthapuram 695 022, India

Crew Module Fairing (CMF) for Pad Abort Test (PAT) of Crew Escape System (CES) is configured and designed with the objective of flight qualifying necessary features like external aerodynamic shape, thermal protection system, along with Escape Motors (namely Low-altitude Escape Motor (LEM) and High-altitude Escape Motor (HEM)), with interfaces simulated as in actual flight. For improving the aerodynamic stability of the vehicle, four grid fins are attached at the aft end of CMF. Interfaces for mounting LEM, HEM, grid fins along with its deployment mechanisms and Crew Module through CM–CES attachment have been provided on CMF.

The design was supported by rigorous analysis, both 2D as well as 3D, of different sub-assemblies and interface joints for the respective critical load cases. To meet the challenges of launch requirements and schedule, the feasibility of combining tests of varying nature has been explored. By meticulous planning of the test scheme, set-up, load cases and instrumentation, and through a judicious combination of test and analysis, structural qualification of CMF could be achieved meeting the mission schedule. CMF has been successfully flown in PAT, as evident from radar monitoring. Post-flight analysis of strain data indicates the integrity and good health of CMF during the entire phase of the mission.

Keywords: Aerodynamic stability, Crew Module Fairing, grid fins, Pat Abort Test.

Introduction

HUMAN spaceflight missions require reliable escape provisions for the crew during all phases of the mission. An unmanned mission, 'Pad Abort Test (PAT)-01' was carried out for demonstrating the capability of the Crew Escape System (CES) to safely eject the Crew Module (CM) from the launch pad in case of any exigency and also assessing the performance of CES, a major critical subsystem in a human-rated launch vehicle. CM Fairing (CMF) is an important part of CES. The primary function of CMF is to protect CM from plume impingement during escape motor firing and from the aerodynamic loads during ascent phase of the flight. In a nominal mission, this is jettisoned along with CES. The loads during ascent phase of the flight are to be transferred to the Launch Vehicle (LV) and Orbital Vehicle (OV) through the fairing. CMF houses the CM which is attached by means of CM–CES structure. It also houses the four High-altitude Escape Motors (HEMs). For improving the aerodynamic stability of the vehicle four grid fins are attached at the aft end of CMF. Interfaces for mounting Low-altitude Escape Motor (LEM), HEM, grid fins along with their deployment mechanisms, CM through CM–CES attachment are provided on CMF. Figure 1 shows the CES flight configuration.

Design of CMF along with the required interfaces for CM, Escape Motors and grid fin has been carried out. This article discusses in detail some major aspects of design and qualification of CMF right from configuration design stage and findings of post-flight analysis of the structure.

Configuration

CMF has a cone–cylinder configuration with overall height of 5.4 m, a maximum external diameter of 3.7 m and a half cone angle of 30°. The fore end (FE) ring of the structure interfaces with the LEM igniter end flange. Unlike conventional payload fairing of a LV for which the primary loading is the external pressure acting on its surface, CMF has to be designed for, in addition to external pressure, a set of heavy concentrated loads due to attachment of four HEMs, CM and four grid fins.

Figure 2 shows the configuration of CMF along with the mounting interfaces provided. Conical panels provide mounting interface for four HEMs and also the CM–CES truss structure which holds the CM. Cylindrical region provides interfaces for grid fins along with their deployment mechanisms. Interfaces for attachment links providing lateral support for CM which were introduced later in the design, are provided in the aft end (AE) ring of CMF. Required cut-outs for CM–CES truss assembly, pyro arming of motors and separation systems, HEM nozzle exits and wire tunnel interfaces are provided in the structure.

*For correspondence. (e-mail: ap_beena@vssc.gov.in)

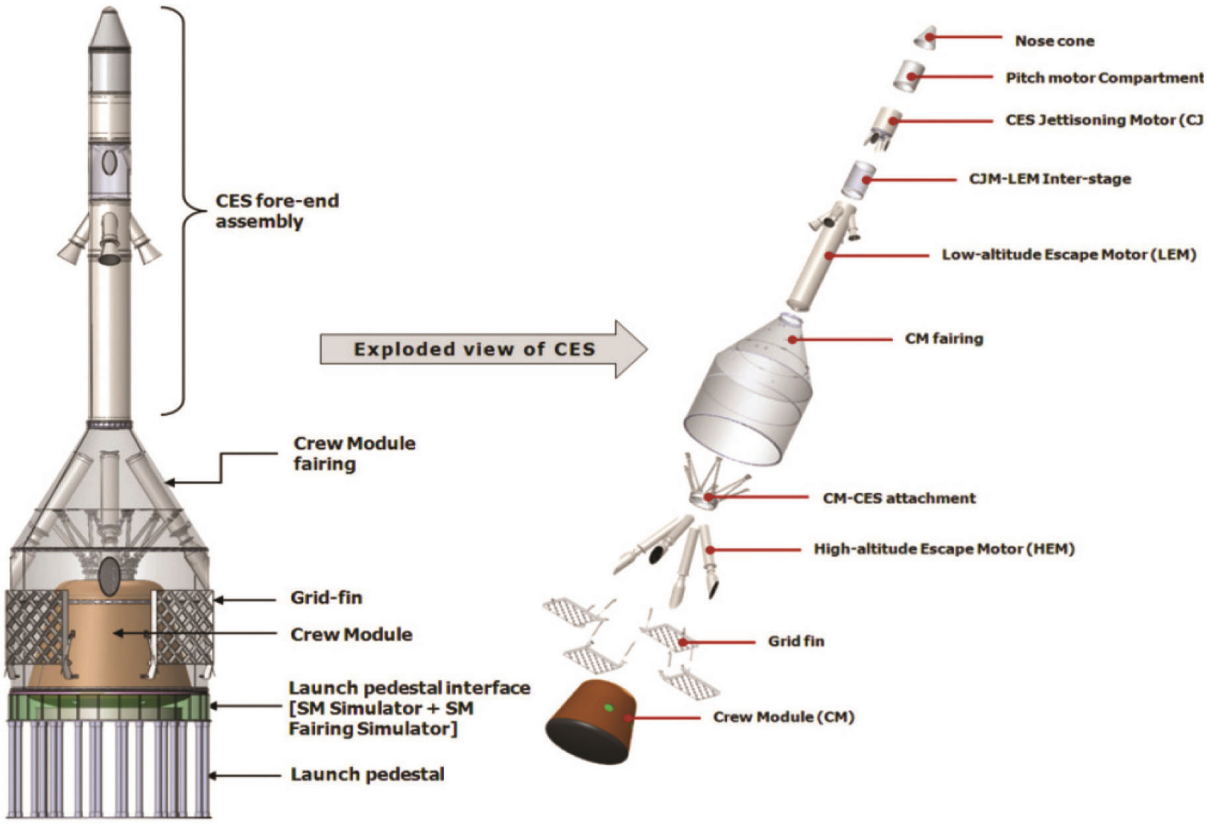

Figure 1. Crew Escape System – configuration.

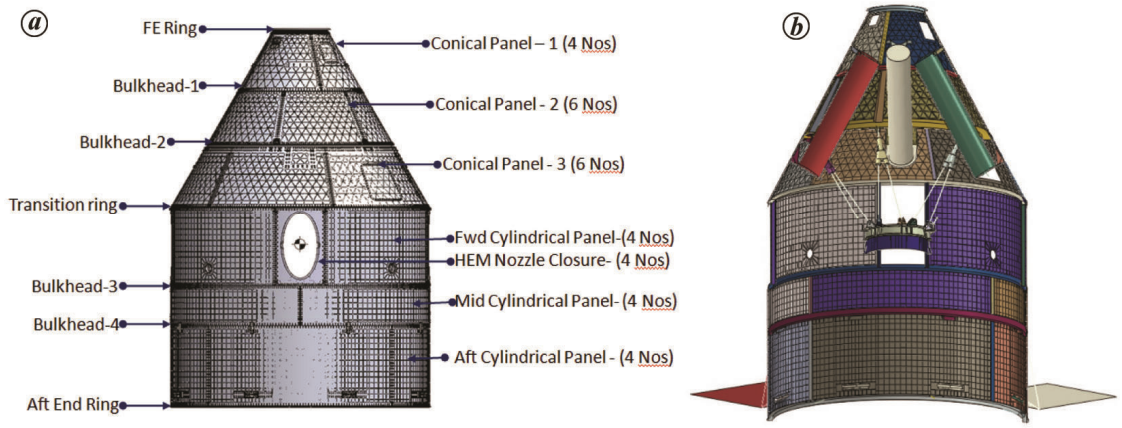

Figure 2. ***a***, Crew Module Fairing (CMF) – external configuration. ***b***, Sectional/internal view of CMF.

Methodology of load estimation

The various loads acting on CES are aerodynamic load that depends on the dynamic pressure and aero force coefficient at a particular Mach number and angle of attack, the thrust force of various motors and inertia loads. Load estimation has been done by the Load Team by adopting the inertia relief approach using a FE model of CES + CM, simulating the mass consumption versus time history of each motor and the total mass, mass moment of inertia and centre of gravity (CG) at any instance. Aerodynamic load distributions are integrated along each element length of the FE model and applied as concentrated forces at the grid points of each element. Thrust (altitude-corrected) on LEM, HEM and Pitch Motor (PM) are applied on the thrust acting points on each motors. The internal forces such as shear force, bending moment and axial force are extracted from the

model. The rigid body loads thus obtained are multiplied with appropriate flexibility factors to arrive at the limit loads at different interfaces.

Design-driven events

The total duration of the PAT mission is around 230 sec. The loading regime for CMF starts from the initiation of the mission with simultaneous ignition of LEM and HEM at T + 0 sec, immediately followed by PM ignition at T + 0.9 sec. After the tail-off of the motors by around 5 sec, CES + CM continues in the coasting phase till CM separation at T + 20 sec, at which the CES Jettisoning Motor (CJM) fires and takes CES away from CM. Out of the total 20 sec flight duration for CMF, the design driving events primarily occur in the thrusting phase of the mission up to 5 sec.

Being first of its kind hardware with several critically loaded interfaces, the design could not be done following the practice of designing for the station loads defined, as is conventionally done for LV structures. Primary loads acting on the structure are as follows:

- External aerodynamic pressure.
- Inertia loads due to self as well as mounted hardware like HEM, grid fin and CM.
- Thrust load of motors.
- Grid fin loads.
- Grid fin deployment loads.

Combinations of the above loads which are critical for different interfaces were judiciously arrived at based on preliminary analyses and engineering judgment. The following load cases were identified to encompass the critical combinations for different interface locations:

(1) Maximum load at LEM–CMF interface (event).
(2) Maximum aerodynamic pressure during the course of the mission.
(3) Maximum HEM thrust load transferred to CMF at HEM attachment interface.
(4) Maximum load at CM–CES truss structure interface (due to CM inertia).
(5) Maximum grid fin loads transferred to CMF at grid fin attachment interface.
(6) Maximum grid fin deployment load at mounting interface.
(7) Maximum CM aft-attachment link load transferred to AE ring of CMF.

Design

Design of the structure has been carried out considering all the critical load cases as mentioned in the previous section. Being a structure subjected to primarily external pressure loading, along with other concentrated loads due to attachments, integrally stiffened construction was proposed. Since the conical panels had to provide interfaces for the mounting of HEMs and CM, isogrid construction was proposed for improved stiffness. Cylindrical shells were proposed to be of orthogrid construction considering the external pressure loading, with the required reinforcements provided for grid fin attachments.

Considering the available sheet sizes, conical as well as cylindrical shells are configured with three panels each, with sheet length in the rolling direction. The bulkhead positions are firmed up in such a way that it provides the required stiffening at attachment locations and cone–cylinder interface, and also ensures stability of the panels. Since the sheet length is aligned in the rolling direction, the height of each panel is limited and panel-to-panel load transfer takes place through bulkheads. Hence joints are designed accordingly. Each conical/cylindrical panel is configured in three or four circumferential segments and connected through longitudinal splice joints.

Preliminary sizing of each isogrid panel has been made using the design formulae provided in the *Isogrid Design Handbook*[1], taking into account external pressure load, axial load and bending moment at the respective interfaces. Considering constraints in rolling, the total depth of panels is kept as 18 mm maximum. For conical panels having lower diameters, rolling feasibility was studied and depth was restricted to 14 and 16 mm for fore end panel and middle panel respectively. Other constraints related to fabrication, in $b\backslash d$ ratio (depth of the rib/dia of cylinder), and skin and rib buckling were also considered in sizing of the isogrid.

Sizing of orthogrid pockets in the cylindrical shell has been made considering the local buckling of pockets as well as global buckling of the shell[2]. Cylindrical panel provides mounting interface for the four grid fins. Necessary stiffening at these locations is provided by means of bulkheads, sector bulkheads and sector brackets, and also by stiffening the orthogrid pockets.

Adequacy of the end rings and bulkheads in withstanding external pressure, bending moment and also loads due to local attachments has been verified using design calculations[3]. The AE ring configuration has been finalized considering the Merman band tension loads. It was later assessed for the CM aft attachment link loads and necessary stiffening provided at the link attachment points.

Grid fins which are held in stowed condition during a nominal mission are deployed by means of pyro thrusters, in case an abort is called for. The pyro thruster is connected to the forward cylindrical panel through an interface flange using fasteners. These interfaces are subjected to pyro thruster loads which are transient in nature and have been reinforced adequately to withstand these loads. Cut-outs provided in the conical as well as cylindrical panels for wire tunnel routing, CM–CES assembly and pyro arming are reinforced by stiffening the pockets

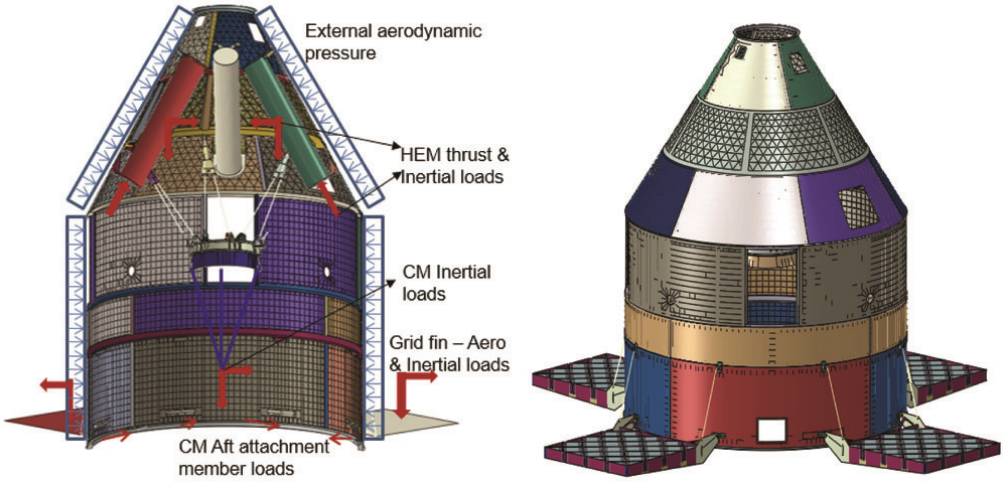

Figure 3. Loads acting on CMF during ascent-phase of Pad Abort Test (PAT).

following the approach given in the *Isogrid Design Handbook*[1]. Picture-frame reinforcement using longerons is done at the cut-outs for HEM nozzle exits.

Preliminary sizing was carried out based on design calculations as well as the 'design through analysis' approach.

Challenges in the CMF design and testing

Unlike payload fairing of a launch vehicle (LV), CMF houses HEMs, provides interfaces to LEMs, and CM through CM–CES truss and CM aft attachment and mounts grid fins externally. These interfaces are subjected to highly concentrated loads, in addition to aerodynamic pressure loads, during an abort mission. Also, transient and shock loads at the grid fin deployment interface and shock loads at CM aft attachment interface pose a major challenge for the design. Apart from loads, cut-outs are to be provided for pyro arming and the CM–CES assembly.

Like for any structure, the design had to be validated through structural qualification tests. Launch schedule imposed major constraints in testing. Designing the tests following the approach of 'qualifying in parts' and arriving at the test load cases, meeting these constraints in such a way that qualification of all critical interfaces could be achieved without any other location being over-tested, was a major challenge.

Analysis

The design was further supported by detailed analysis, both 2D as well as 3D, of different sub-assemblies and interface joints for the respective critical load cases. Different FE models have been employed for the analysis of flight and structural test cases:

(i) Global model of CMF integrated with grid fins, HEMs and CM–CES truss members along with CM–CES ring to simulate all the critical flight events. Buckling analysis was carried out using this model for identified critical events during flight.

(ii) Two-dimensional axisymmetric as well as 3D solid model of the CMF to LEM interface joint.

(iii) A 45° sector 3D model of forward cylindrical panel for nonlinear transient structural analysis of pyro thruster interface for grid fin deployment load.

(iv) Integrated model of cylindrical panel along with grid fin/simulator, with damper and hinge interfaces simulated (45° sector).

Structural analysis for ascent-phase loads

The FE model consisting of solid, shell and beam elements was used for analysis (Figure 3). The model includes CMF cylindrical and conical panels, inner rings/bulkheads, splicers, stringers, HEMs, and grid fin modelled using shell elements. Damper and CM–CES truss rods are modelled using truss elements. CM–CES ring and CM–CES attachment brackets and adaptors are modelled as solid elements. HEM propellant mass (corresponding to each load case) was lumped equally at two points, Head-end and nozzle-end interface of HEM to CMF. In the FE model translations are constrained at the LEM–CMF interface fastener locations.

At any instant, loads acting/getting transferred on CMF are HEM thrust loads, self-inertia loads, grid fin loads, aerodynamic pressure and loads due to CM inertia. The challenge in the analysis was to arrive at the combination of the above loads to be applied to match those at each interface specified by the Load Team. These were arrived at based on several iterations. Static structural and buckling analysis was carried out for each critical case by

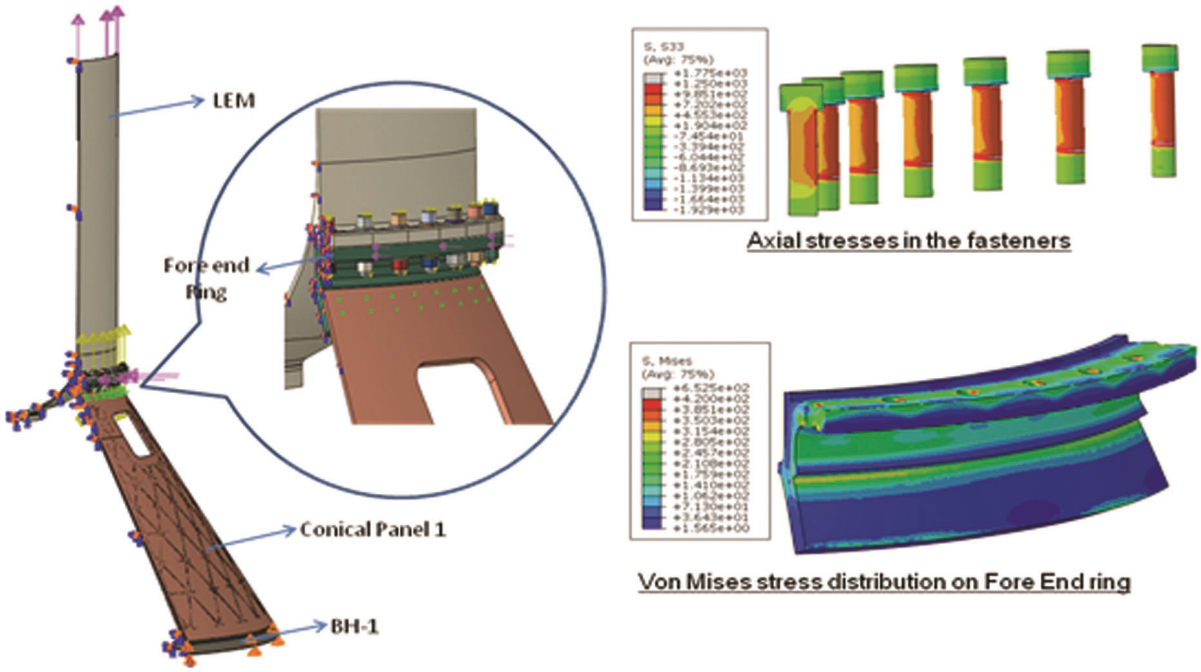

Figure 4. Three-dimensional model details of CMF–Low-altitude Escape Motor (LEM) interface and finite element (FE) analysis results.

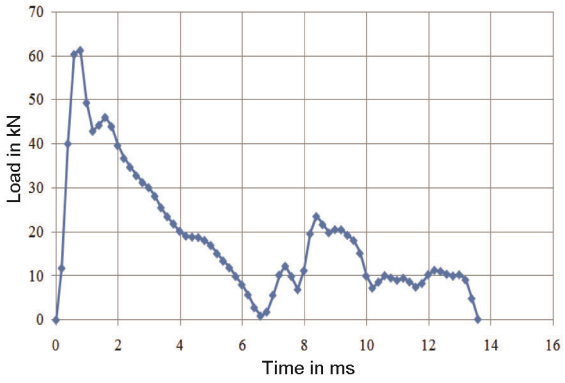

Figure 5. Load–time curve at CMF pyro interface.

applying loads corresponding to each identified critical case.

Minimum margin against buckling obtained from the analysis was 0.49 (with knock-down factor of 0.65). Minimum margin for flight ultimate loads available on the structure was 0.13 w.r.t. proof strength (PS) on the aft end ring. For joints in the structure, the minimum margin was 0.08 w.r.t. PS on Jo Bolts in the aft end ring to aft cylindrical panel.

Analysis of CMF–LEM interface

The igniter end of LEM is interfaced to the FE ring of CMF by flanged joint with bolt and nut assembly. A 45° sector model consisting of the FE ring, motor interface flange and shell, forward conical panel (Cone-1) and bulkhead-1 was considered for analysis. The model includes the pyro arming cut-out in the forward conical panel (Figure 4). For the interface between the fore end ring and LEM, fastener preload and contact between the two flanges are simulated. Cyclic symmetry condition is applied on either side and axial constraint is applied on the aft end of bulkhead-1. Radial deflection of LEM flange due to internal pressure is applied on the motor flange thickness. Equivalent axial load (EAL) is applied as force on LEM.

FE analysis results showed that stresses on interface fasteners and FE ring are within design limits.

Nonlinear transient analysis of pyro thruster interface for grid fin deployment load

During deployment of the grid fin upon pyro thruster firing, reaction load will act on the Fairing. The pyro thruster load monitored at the grid fin simulator interface using dummy grid fin test was provided for analysis. Figure 5 shows details of the interface of pyro assembly to CMF.

Combined material and geometric nonlinear transient analysis of forward and mid-cylindrical panel along with the pyro thruster attachment bracket is carried out using a local 45° sector 3D solid model for the specified load history. As shown in Figure 6, fasteners connecting pyro thruster to the cylindrical panel and those in the bulkhead interface have been modelled in detail.

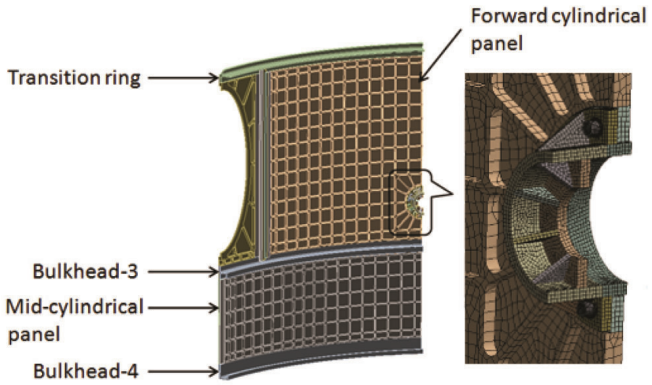

Figure 6. Details of 3D FE model used for transient analysis of CMF pyro interface.

Analysis indicated large deflection of the order of 60 mm in the panel and localized plastic strains in the ribs. This called for stiffening of the panel near the pyro interface. Stiffening scheme was worked out based on the above analysis and implemented in the hardware.

Integrated analysis of cylindrical panel with grid fin simulator

FE analysis of global shell model of CMF indicated that there is a local region of high stress concentration on CMF at grid fin damper bracket interface. To assess and quantify the stresses, detailed 3D modelling of the damper bracket interface including cylindrical panel bulkheads and AE ring was carried out considering 90° symmetry (Figure 7). All interfaces are simulated using contact elements. Geometric and material nonlinearities are considered for FE analysis. Preload on the fasteners are simulated using pre-tension elements. FE results showed yielding occurring on CMF panel at grid fin damper bracket interface near to bolt hole locations, based on which the interface was locally reinforced.

Structural qualification tests

During ascent phase of the flight, the aft end ring of CMF is in free condition (unconstrained/no structure interface) with the inertia forces (self as well as mounted components), external pressure, grid fin loads and HEM thrust loads acting on the CMF getting reacted at the LEM interface. Ground test simulation of loads acting as in flight, was extremely challenging and involved, considering the constraints in testing due to schedule constraints.

Analysis was carried out using the integrated model of CMF with grid fin, HEM and CM–CES Truss members along with CM–CES ring and the critical test load cases were arrived at as follows:

(i) CM–CES truss fore end interface qualification by simulating maximum EAL and HEM thrust transfer interface qualification by simulating maximum thrust loads in the same load case.
(ii) LEM–CMF interface qualification by simulating fastener load distribution as in flight along with maximum EAL.
(iii) Maximum CM aft attachment link loads (tension and compression) simulation along with preflight aft attachment link load distribution and grid fin loads.
(iv) Grid fin interface qualification by simulation of preflight estimated maximum grid fin loads along with CM aft attachment load distribution for the same instant during flight.

To facilitate completion of the tests meeting the launch schedule, the following constraints were imposed by the testing agency:

(i) Available fixtures to be used to the extent possible.
(ii) LEM interface was simulated by means of mild steel (MS) adapter.
(iii) Application of external pressure during test was not feasible in the specified time frame.
(iv) Integrated test of CMF with CM was not feasible. Hence a spider web-like fixture simulating CM stiffness had to be used.
(v) Point of application of CM inertia load had to be offset from the actual CG location by around 1 m.
(vi) Integrated test of CMF with actual grid fin was not feasible due to non-availability of hardware and constraints in load application on the grid fin. Grid fin simulator had to be used.
(vii) Grid fin load was proposed to be applied at the CG location which was offset from the actual Centre of Pressure (CP) location. Also, moments acting at the grid fin CP location had to be simulated through equivalent forces.

To determine the adequacy of the test fixtures/loading adaptors along with grid fin simulators and to ensure load distribution in the hardware as in flight and to rule out over-testing of any component, rigorous analyses were carried out using an integrated model with test fixtures. Figure 8 shows loads applied in the FE model to simulate structural test conditions.

Grid fin simulators and loading adaptor along with interfaces are modelled as shell elements and damper simulator rods as well as CM aft attachment member are modelled as truss elements.

Studies on Crew Module stiffness and location of load application

CM during flight is attached to CMF through the CM–CES truss structure with lateral support provided at the

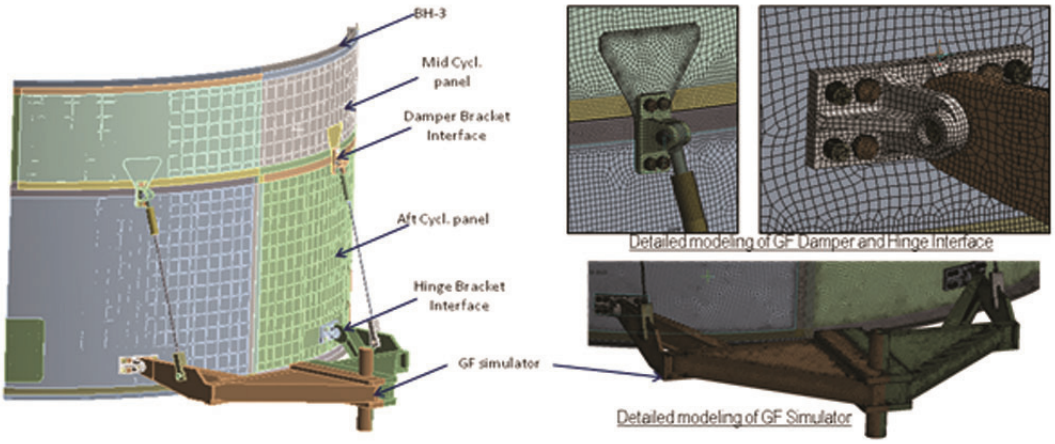

Figure 7. Three-dimensional FE model of CMF–grid fin simulator interface study.

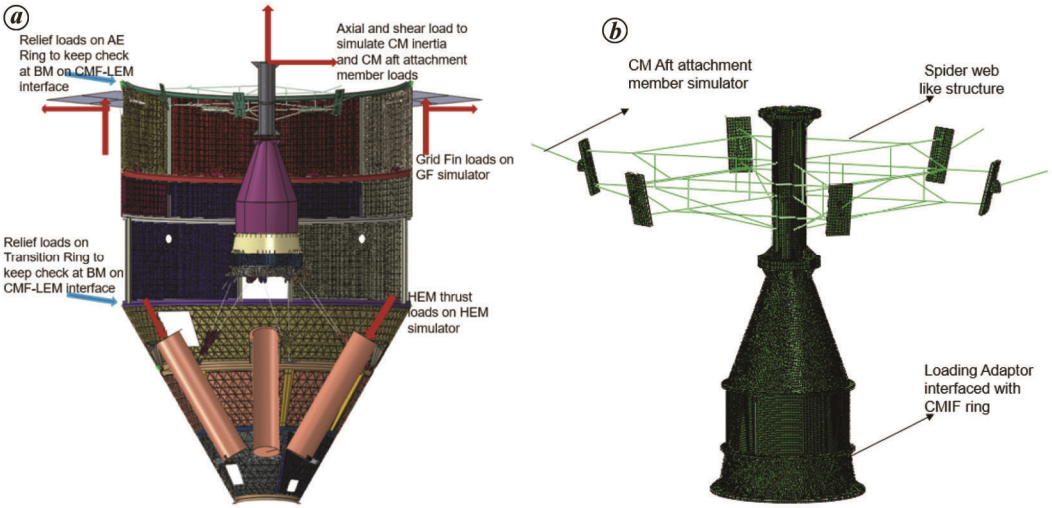

Figure 8. ***a***, Loads applied in FE model to simulate structural test conditions. ***b***, Loading fixture with spider web-like structure.

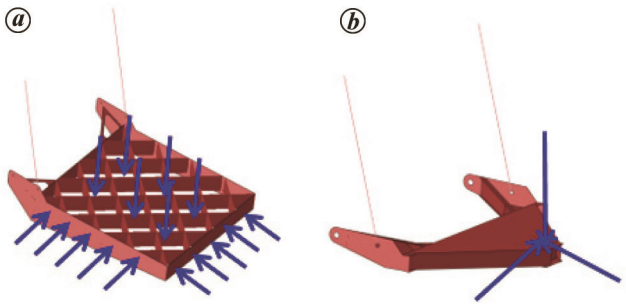

Figure 9. ***a***, Pictorial representation of aerodynamic loads acting on grid fin. ***b***, Loads applied on grid fin simulator.

aft end by means of six radial links connecting the dome interface ring of CM to the AE ring of CMF. Adequacy of the spider-like fixture in simulating the CM stiffness was verified through analysis and required modifications suggested in the fixture, such that the aft link loads are simulated as in flight. Sensitivity of the stiffness of CM stiffness simulator to link load distribution studied was found to be benign.

Studies on adequacy of grid fin simulator

Grid fin simulator was configured to have stiffness comparable to that of the composite grid fin.

Aerodynamic loads acting on the grid fin during flight are provided as forces and moments acting at the CP location. Figure 9 gives pictorial representation of aerodynamic loads acting on grid fin and loads applied on Grid Fin Simulator during structural test. Since moment simulation is not feasible in the test-setup, loads to be applied on the grid fin simulator, to simulate the grid interface loads as in flight was worked out and applied for structural test.

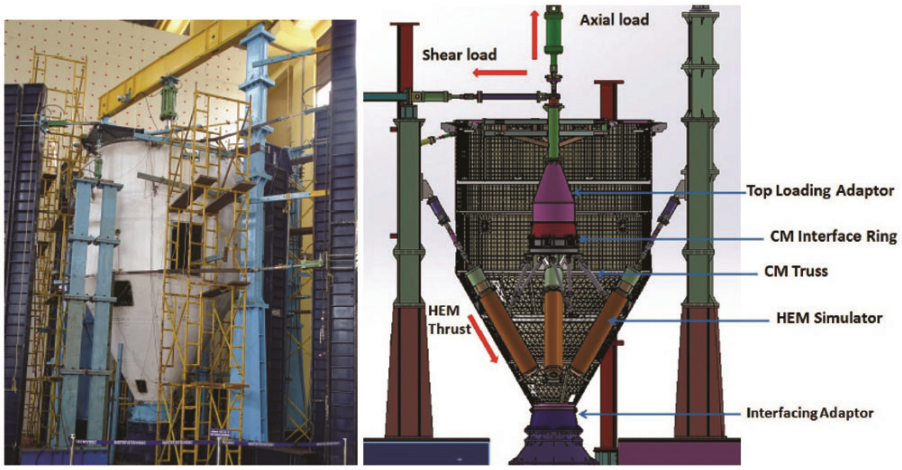

Figure 10. Structural qualification test set-up and the schematic of load application.

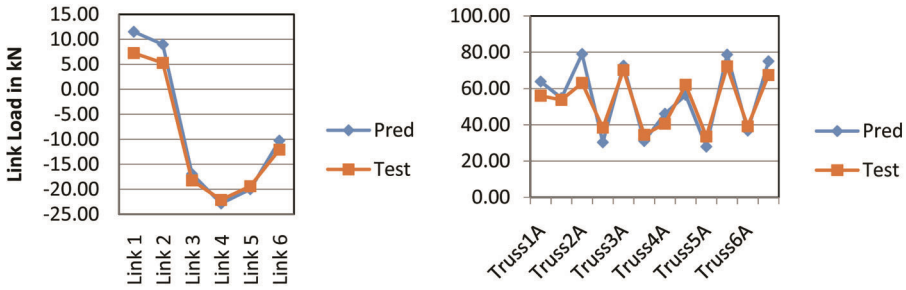

Figure 11. CM aft attachment link load and CM truss member load comparison between test and prediction for a typical load case.

Studies on LEM interface stiffness

FE analysis was also carried out to have comparative study of fastener load distribution at LEM–CMF interface for flight case as well as for the proposed structural test wherein a LEM simulator is used in place of LEM. FE analysis showed that the test closely simulates the flight condition.

Studies on implication of non-application of pressure

Since pressure load is not applied during test, equivalent load had to be distributed at the available loading interfaces such that net reactions at the required interfaces are matching with the requirements. Also, the grid fin loads to be applied in the test were augmented to account for non-application of moments, which also contributed to an imbalance in the interface loads. This had to be compensated by applying relief loads at the available loading interfaces.

Considering the above constraints and based on rigorous analysis, an acceptable test scheme was developed and the critical test load cases and the load combinations to be applied during the test were arrived at such that each interface is subjected to its respective qualification loads, ensuring that loads at any other location do not exceed the design limits. Since the hardware is intended for flight, the proto-flight testing approach been adopted, i.e. structural tests are conducted for 1.15 times the limit load.

Structural qualification test and observations from post test analysis

For structural test, the test hardware is inverted and fore end ring of CMF assembled to the bottom interface ring/adaptor through which applied load is transferred to the ground. Figure 10 shows the actual test set-up and the schematic of load application. Four HEM simulators are assembled to the hardware to apply thrust load. Loading adaptors and spider assembly are assembled to the CM attachment ring to simulate inertia load (tensile). Four grid fin simulators are assembled to the test hardware to apply grid fin loads. In grid fin simulators, radial and tangential loads are applied as a resultant lateral load and axial loads are applied separately. Lateral loads on CMF are applied in three planes: (a) through a loading adaptor connected to the spider assembly; (b) directly at AE ring, and (c) directly at the transition ring. Shear wall and

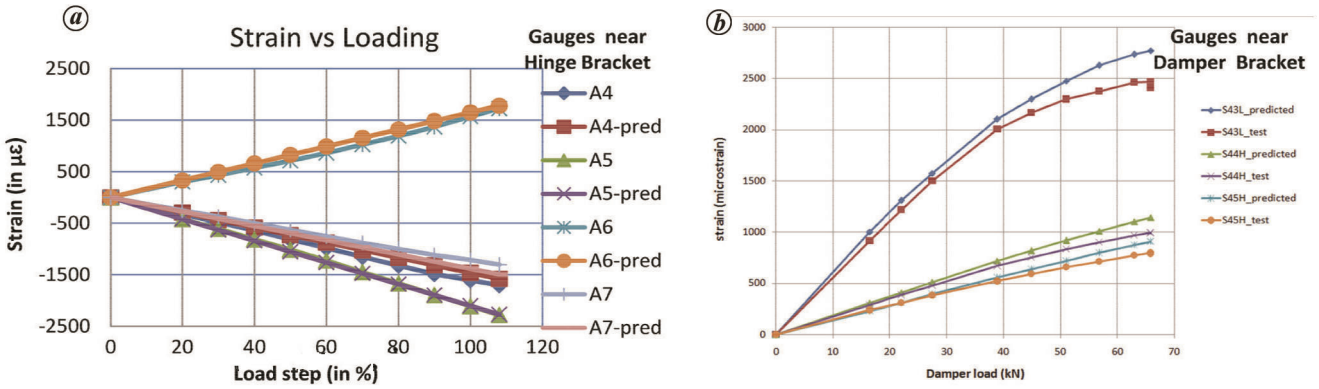

Figure 12. ***a***, Comparison between test measured and predicted strain values for gauges near hinge bracket interface. ***b***, Measured and estimated strain from nonlinear FE analysis for damper load.

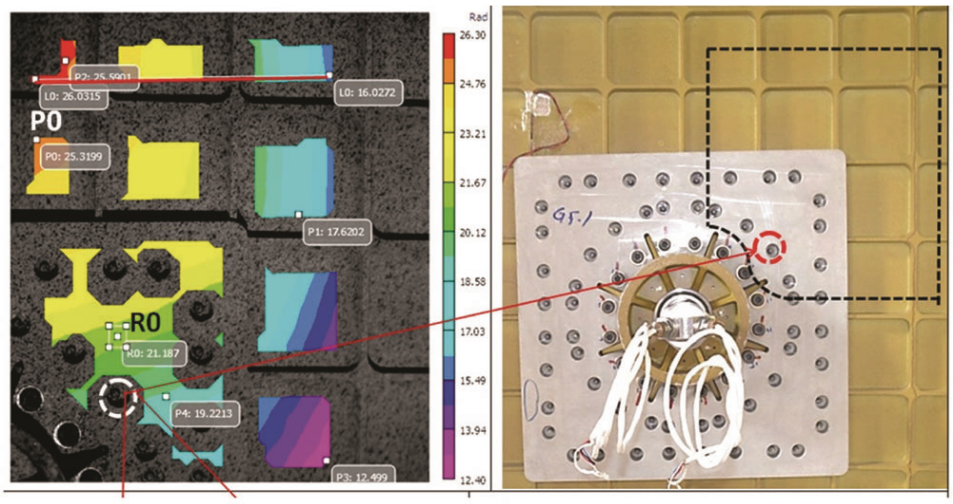

Figure 13. Total deformation of the panel measured using digital image correlation during deployment test.

portals is used to apply the lateral load. Base beams and columns are mounted on the base to apply HEM thrust, axial loads and grid fin loads.

Structural test was carried out for all the identified test load cases and the hardware successfully withstood the same.

For on-line monitoring of the health of the hardware during the course of structural testing and for a comparison between analytical and structural test results in order to validate the structural design and analysis methodology, detailed instrumentation scheme was worked out covering all critical locations on CMF. All CM truss rods and grid fin damper rods were strain-gauged. Load cells were provided to monitor the attachment link loads. Overall, 148 strain gauges and 26 displacement transducers (DTs) were used.

In general, strain gauges along with grid fin damper loads, CM aft attachment member loads and CM truss member loads are found having good agreement with prediction for most of the load cases (Figure 11). However, during grid fin interface qualification test case, there was mismatch in predictions for gauges near damper rod and w.r.t. the test measured values. This gap was bridged using local 3D FE model analysis (Figure 12).

Grid fin deployment test

As a part of the qualification of the deployment system along with CMF and composite grid fin, grid fin deployment tests were carried out. During the first test, debond was observed in the composite grid fin near the pyro attachment region. Subsequently, the grid fin was stiffened and the modified grid fin was subjected to deployment. Strain gauges were provided at critical locations and digital image correlation (DIC) was employed for displacement measurement at the loading interface (Figure 13). Reaction force on the structure during deployment was also measured.

Analytical predictions for strains and displacements were made based on nonlinear transient analysis for the measured reaction force with zero damping and compared with test data.

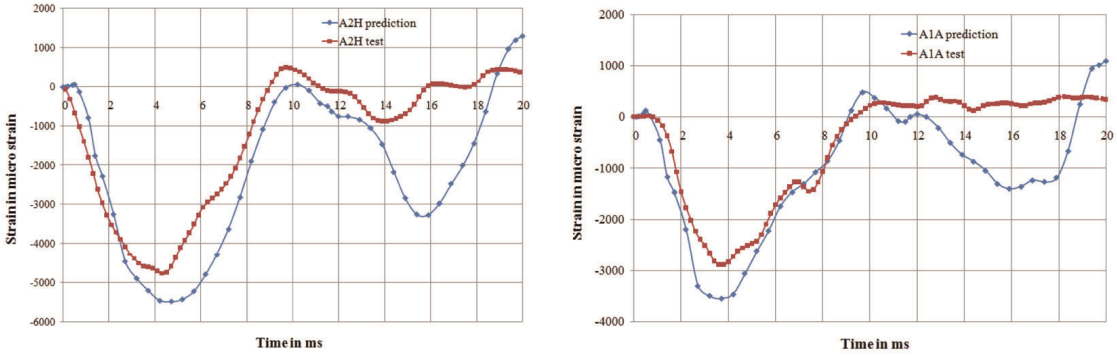

Figure 14. Strain data comparison between test and prediction at typical strain gauge-mounted locations for grid fin deployment test.

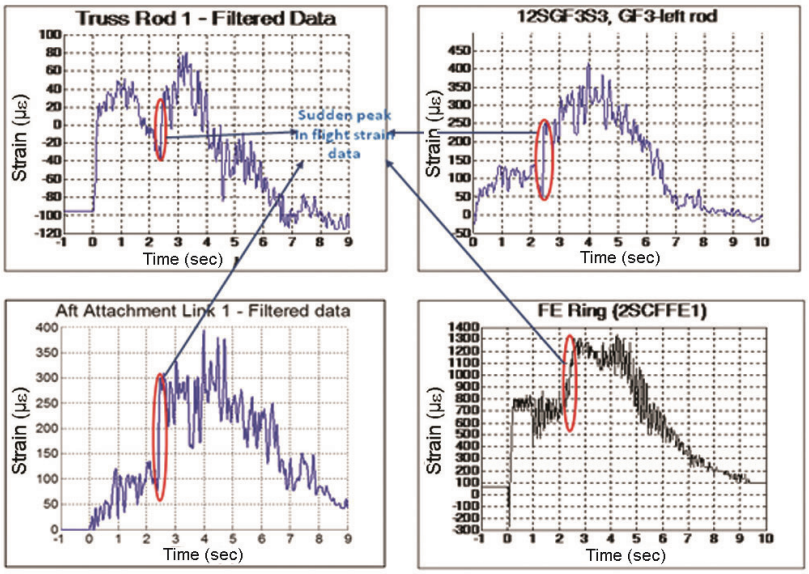

Figure 15. Flight strain data showing sudden peak at 2.38 sec at different strain gauge-mounted locations.

The maximum value of deformation obtained using DIC is around 26 mm, whereas deformation at the respective point using FE analysis is around 31 mm. Figure 14 shows the comparison of strain gauge response comparison to the transient loading between test and prediction at typical strain gauge locations.

Fair match is observed between measured and predicted values of strain gauge locations on the outer surface.

Observations and inference from CM flight data

To monitor the health and assess the loads on different subsystems of CMF, during flight strain gauge instrumentation was done at critical locations. Strain gauge mounting locations were identified such that they meet the objectives of estimating member loads of different subsystems. Gauges were provided on grid fin Damper rods, CM truss rods and locations on CMF where load transfer from these subsystems to the Fairing takes place. Some of these locations were monitored and characterized during structural testing phase and load factors to estimate the loads were established.

In general, flight strain data as well as on-board and tracking cameras indicated the integrity of CMF and CES structures. The noise in the strain data was filtered using the low-pass filter, filtfilt function of Matlab, which allows filtering of data without any phase shift. The filtered data alone were used here for load estimation. Summary of the observations and assessment on loads on different subsystems is as follows.

Most strain channels followed the trend expected during burning and after burnout of the motors. However, in most channels, a sudden peaking/shooting of magnitude is observed at T0 + 2.38 sec (Figure 15), which was not expected as well as predicted during pre-flight estimation of loads.

The strain gauge channels on HEM nozzle end bracket follow expected trend of HEM thrust profile as shown in Figure 16.

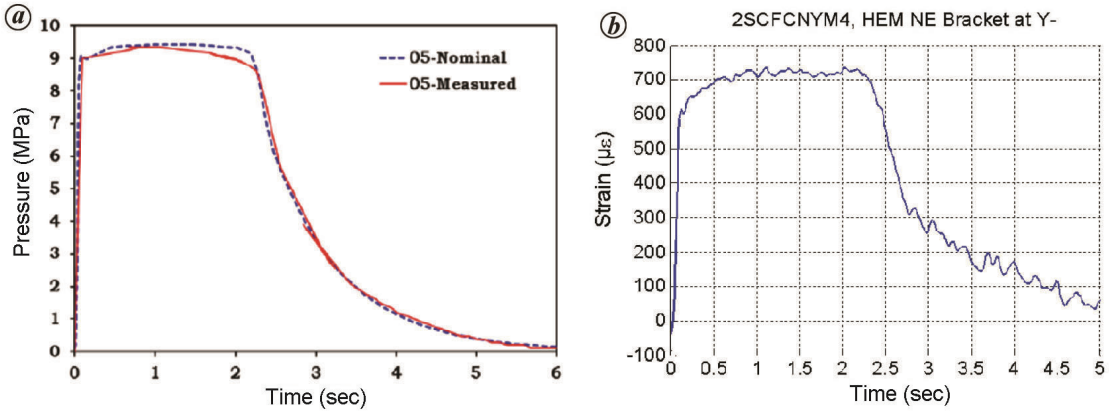

Figure 16. ***a***, Flight measured HEM thrust profile versus prediction. ***b***, Strain gauge mounted on HEM nozzle end bracket following thrust profile.

Table 1. CM-CES Truss loads estimated from flight strain data at different time instant

		With zero correction (load in kN)				
Truss rod ID	0 sec	1.5 sec	2.1 sec	2.5 sec	3.2 sec	5 sec
1	–19.5	25.9	18.7	27.2	30.1	10.6
2	–7.8	41.9	44.0	44.7	34.6	17.6
3	–15.6	33.2	29.7	33.8	24.3	7.7
4	–7.8	33.3	39.0	38.0	25.2	13.3
5	–15.6	51.7	54.7	61.5	44.6	19.9
6	–7.8	45.3	40.8	46.0	41.4	20.1
7	–19.5	42.1	44.7	54.3	33.8	16.6
8	–11.7	34.5	33.3	35.9	37.0	12.6
9	–15.6	43.9	39.9	48.1	33.8	14.7
10	–11.7	31.1	24.2	26.7	36.4	10.9
11	–23.4	51.8	46.3	57.3	56.6	25.0
12	–15.6	47.5	44.9	51.3	49.2	20.9

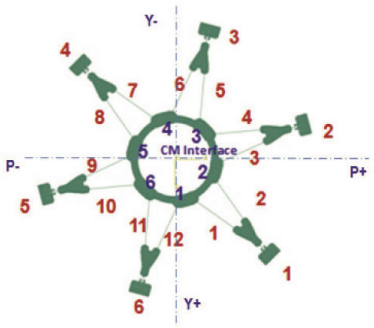

Figure shows the orientation of truss rods w.r.t. the Pitch & Yaw axes

Strain gauge readings during flight are expected to be lower than the structural test value since during structural test, there is no external pressure application, and external pressure will try to compensate the HEM thrust.

Assessment of the CMCES truss rod loads. During pre-flight instrumentation, each truss member was provided four gauges equidistant circumferentially on the rod. In Table 1, before the ignition of the motors, all truss rods showed negative strains; hence load estimated at different time intervals was updated with zero correction. Load factor worked out during structural test was used to estimate truss loads. Peak truss load of 66.3 kN observed in flight was 8.7% higher than pre-flight maximum truss rod load estimate of 61 kN. In general, truss loads observed are higher than pre-flight limit loads.

Assessment of the CM aft attachment links. During structural test of CMF with Link Assembly, a spider assembly simulating CM stiffness and dummy links was used. Loads on the link were measured using load cells. Hence calibration data for CM aft attachment link load are not available. As part of flight instrumentation, a coupler on CM aft attachment link was strain-gauged using a single strain gauge. To assess the load factor (kN/$\mu\varepsilon$), FE analysis of coupler was carried out under uniform load. Peak aft attachment link loads estimated based on load factor using flight-measured strains are significantly higher than pre-flight load predictions. Since only single strain gauge measurement was available on coupler (component of CMF link assembly), probability of having bending component in load estimation cannot be ruled out.

Assessment of the grid fin damper loads. Based on the load factor (kN/μ) established for damper rods during structural test, damper loads are estimated for the flight at $t + 4$ sec (Table 2). Preflight estimate of maximum damper load was 81 kN. Damper load worked out from the flight strain data from strain gauges mounted on damper rods are much higher in comparison to pre-flight estimate.

Also, the strain gauge channels on damper rod show sudden jump in strains at 2.38 sec. However, the channels follow the predicted trend of damper rod loads peaking/increasing after the motors burn out (Figure 17).

Due to uncertainty in the damper load, data from strain gauges mounted on the CMF near to damper interface

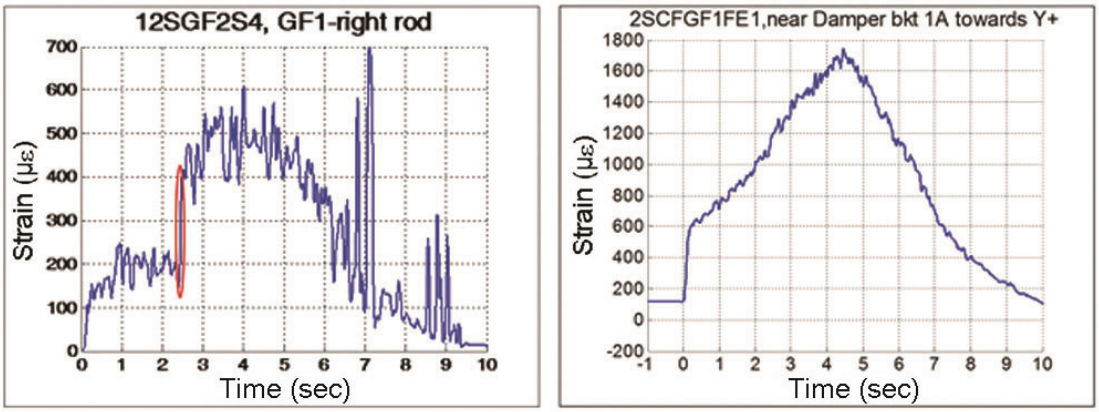

Figure 17. Flight strain data for strain gauge-mounted on grid fin damper rod and on CMF just above the same grid fin damper bracket.

Table 2. Grid fin damper loads estimated from flight strain data (measured on grid fin damper rod)

Damper ID	GF1-LH	GF1-RH	GF2-LH	GF2-RH	GF3-LH	GF3-RH	GF4-LH	GF4-RH
Damper load (kN)	121.2	131.1	74	173.4	95.2	84.4	121.2	125.2

Table 3. Grid fin damper loads estimated from flight data (measured on CMF above grid fin damper bracket interface)

Damper ID	GF1-LH	GF1-RH	GF2-LH*	GF2-RH	GF3-LH	GF3-RH	GF4-LH*	GF4-RH*
Damper load (kN)	56	87.2	65.2/76.7	56.2	62.4	59.2	45.1/53.1/87.8	40.4/47.0/64.5

*For these grid fin damper rods, strain gauges were not provided during the test and hence damper loads are worked and from identical locations from structural test.

which were also part of structural testing, were compared with the test data and damper loads were correlated (Table 3).

Damper load worked out based on flight-measured strains in CMF were comparable to the pre-flight estimate. Since loads computed for most of the systems of CMF were found to be higher than pre-flight estimates, it was recommended to have a revisit on the pre-flight loads/co-efficients and load estimation methodology.

Conclusion

Design and analysis of the CM Fairing which is a first of its kind hardware with several critically loaded interfaces was carried out meeting the project specifications and schedule. Cone–cylinder configuration with integrally stiffened construction-isogrid in conical shell and ortho-grid in cylindrical shell portions was proposed, based on the nature of loading in the respective areas. A judicious combination of integral stiffening as well as stringer stiffening provided for cutout reinforcements and stiffening required near local attachments. By meticulous planning of the test scheme, set-up, load cases and instrumentation, and through a judicious combination of test and analysis, structural qualification of CMF could be achieved meeting schedule. Proto flight testing approach was adopted. CMF has successfully flown in the PAT mission. Post flight analysis of strain data indicates structural integrity of CMF during the entire phase of the mission. However, loads worked out from flight measured strain data, especially, the grid fin damper loads and CM-CES truss loads are found to be higher than the pre-flight estimated loads.

1. *Isogrid Design Handbook*, NASA CR-124075, February 1973.
2. *Analysis and Design of Flight Vehicles Structure*, E. H. Bruhn.
3. *Shigley's Mechanical Engineering Design*, 8th edition.

ACKNOWLEDGEMENTS. We acknowledge the support and valuable guidance provided by Dr S. Unnikrishnan Nair (Director, HSFC) and P. Sunil (Group Director, HTDG). S. Sirajudeen Ahmed (Group Director, Structural Design and Engineering Group, VSSC) and Isac Daniel (Group Director, Structural Testing Group, VSSC) towards timely completion of the above activity.

doi: 10.18520/cs/v120/i1/129-140